Breaking moraine dams by catastrophic erosional incision

Rachel Zammett

March 15, 2007

1 Introduction

Glacial lakes occur in many mountainous areas of the world, such as the European Alps or the Cordillera Blanca mountain range in north-central Peru. Here we consider those glacial lakes that were formed during the period of glacier retreat that followed the end of the Little Ice Age (figure 1). Such lakes are typically up to a kilometre long, hundreds of metres wide and up to a hundred metres deep and are often dammed on at least one side by moraine (sediment deposited by a glacier).

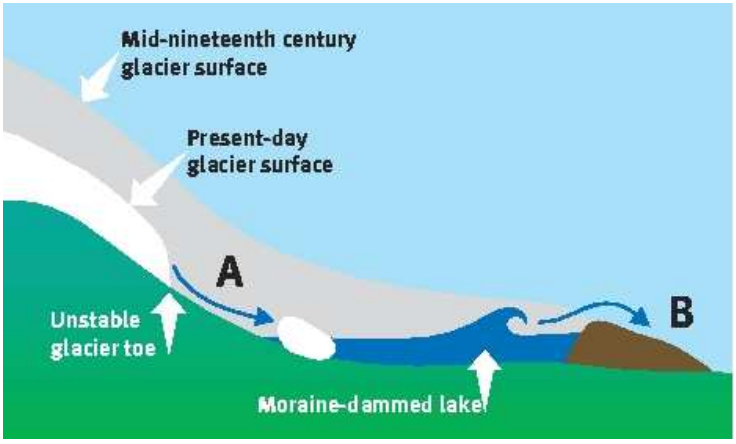

Figure 1: Schematic diagram of a glacial lake, taken from Clague and Evans [2]. The upper (grey) glacier surface is that of a long, thick glacier that would have advanced during the Little Ice Age. When this period of cool climate ended, glaciers retreated rapidly and substantially; such a thin, retreating glacier is labelled 'modern day glacier'. It is during a period of glacier retreat that a glacial lake is typically formed. The moraine dam is shown at the right of the picture. If the toe of the retreating glacier (which is often unstable and heavily crevassed) suddenly deposits a large amount of ice into the lake, a displacement wave which can overtop the dam is initiated.

Moraine dams fail in two main ways. As glacial lakes are often located in steep alpine

valleys (where avalanches and rockfalls are common), or beneath the unstable toe of a retreating glacier, there is the possibility that a large amount of ice or rock may suddenly fall into the lake. This initiates a displacement wave: one such rock avalanche in Peru deposited $O(10^6)$ m^3 of rock in glacial lake Safuna Alta, and initiated a displacement wave estimated to be over 100 m high [8]; more generally, it is estimated that avalanches typically create displacement waves up to 10 m high [4]. Such a displacement wave can overtop the moraine dam and erode its downstream face.

In general, however, we have seen experimentally that one such overtopping wave does not cause the dam to fail. Instead, we observed that some of the initial wave is reflected back into the lake, leading to the formation of a seiche wave (a standing wave in an enclosed, or partially enclosed, body of water). Such waves are often observed to occur naturally in harbours due to tidal influence, for example [13].

The subsequent reflected waves can also overtop the dam, and it is these repeated overtopping events and associated erosion of the dam that lead to the incision of a channel on the downstream face of the dam. If such a channel is eroded to a sufficient depth quickly enough, it becomes a conduit through which the lake can drain; it is this mechanism of lake drainage that we term 'catastrophic erosional incision'.

Evidence for more than one overtopping event has been seen in several such drainage floods [9], and the possibility of a 'series' of waves was identified by Costa and Schuster [4]. The only mention in the literature of a seiche wave in connection with dam failure is found in Hubbard et al. [8], where examination of a moraine dam after a rockfall-initiated displacement wave indicated at least ten reflected waves. We show here how the reflected waves play a crucial role in the failure of the dam.

The other mechanism by which a moraine dam can break is that of gradual overtopping, whereby the lake water level slowly increases until the water overtops and then breaches the dam. Such a water level rise can be caused by excessive snowmelt or rainfall: the moraine which dammed Lake Tempanos in Argentina failed in the 1940s due to meltwater accompanying a 350 m glacier retreat [16].

Drainage of a glacial lake can release $O(10^6)$ m^3 of water and have a peak discharge of 10^3–10^4 m^3 s^{-1} [2]. As the subsequent floodwater moves down valley, it entrains sediment and can form a debris flow. One such debris flow, initiated by a glacial lake flood in Peru in 1941, devastated the city of Huaraz, killing over 6000 people [5]. While the majority of such floods occur in remote, uninhabited valleys, these locations are now often considered for recreation, tourism and as sites for hydro-electric power stations, for example. Thus understanding the hazards associated with such a flood is of prime importance.

In this project, there are two main issues we will address. Firstly, we shall consider the threshold behaviour of the phenomenon - why didn't the moraine dam break in the case of Laguna Safuna Alta, despite an initial wave 100 m high and at least ten subsequent seiche waves? We also consider how to estimate the peak discharge from such a catastrophic drainage event, as this can be used as a measure of how destructive the resulting flood will be.

2 Experiments

We performed a series of experiments over the summer, both as a qualitative exploration of the phenomenon and to quantify some of the theoretical results outlined in Section 3 below. In all cases we used the experimental setup shown in figure 2: a rectangular glass tank with length 125 cm, width 20 cm and depth 30 cm. This was open at one end (the right hand end in figure 2), so that sediment and water could drain from the tank. At the open end, we built a sediment dam. This dam was approximately 10 cm high and 40 cm wide at the base and was made using a mould to endeavour to keep the dams uniform in shape. The tank was then filled with water, and the experiment was left until water had seeped through the entire dam. A single wave was then initiated at the left hand end of the tank; this was to simulate the displacement wave initiated by a rockfall or avalanche.

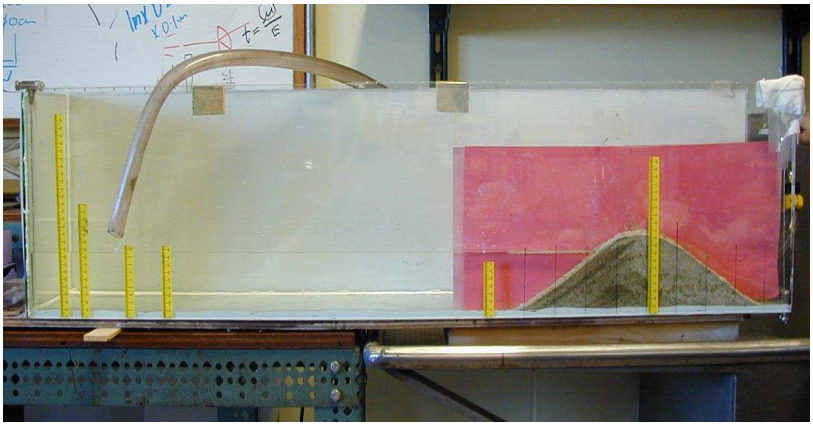

Figure 2: Experimental setup.

Sediment properties

We used four different sediments in the dambreak experiments. These were grit and three types of sand with different particle size distributions. The properties of these sediments (when dry) are summarised in Table 1.

Glacial moraine is characterized by a wide range of particle sizes, from fine clays to large boulders. This sediment is poorly sorted and loosely consolidated; lake drainage typically occurs by seepage through the dam. Clarke [3] shows an example of moraine from Trapridge glacier with a bimodal particle size distribution; this is a feature of many moraines. In order to reproduce such a bimodal particle size distribution, we therefore made two mixtures of sand and grit. The properties of these mixtures (when dry) are summarised in Table 2.

The sediments and their properties will also be discussed in Section 3 below, where we consider the erosion of the dam.

Sediment	ρ (10^3 kg m^{-3})	Porosity	Repose	Modal particle size (μm)
Caribbean Sand	N/A	N/A	N/A	250
Florida Sand	2.34	0.38	39°/34°	310
Beach Sand	2.34	0.35	40°/33.5°	950
Grit	2.42	0.42	37°/28°	1150

Table 1: Properties of individual sediments when dry. Sediment density was calculated from the weight of a given sediment volume once the sediment porosity was determined. Sediment porosity was measured by measuring how much water was absorbed by a given volume of sediment. The column headed 'Repose' shows the angles of repose of the dry sediment; the first value is the angle of repose associated with tilting a pile of sediment, the second that associated with creating a conical pile of the sediment. The differing values are due to the bistability of the system [11]. Modal particle size was estimated from particle size distributions which were obtained by laser diffraction. Some of the properties of the Caribbean sand were not determined.

Mixture	Composition	ρ (10^3 kg m^{-3})	Porosity	Repose
1	Caribbean Sand/Grit	2.38	0.32	38.5°/33°
2	Florida Sand/Grit	2.36	0.37	44°/34°

Table 2: Properties of sediment mixtures, determined as in Table 1. As the mixtures are bimodal by design, we have omitted the modal particle size column.

2.1 Results

Here we consider results from qualitative experiments. We first consider the results of experiments using the individual sediments, some of which are shown in Table 3. We see that grit alone makes a poor dam - its high porosity means that the lake drains out rapidly, and thus makes the dam unstable. It is also difficult to incise a channel in the downstream face because overtopping water simply seeps into the dam rather than eroding it. In contrast, the sands are, in general, better in terms of ease of channel incision. However, they are also prone to slumping when wet, indicating that they would make a poor dam; sand dams were occasionally observed to break before a wave was initiated.

Some of the results for the sediment mixtures are shown in Table 4. Although it is not clear from this table that dams constructed from the sediment mixtures were easier to break by catastrophic incision than those made from the individual sediments, they were qualitatively observed to be better in terms of both initial dam stability and ease of channel incision. These observations lead to the conclusion that it is perhaps the composition of moraine that leads such dams to fail via catastrophic erosional incision - the distribution of particle sizes both increases the dam stability, making the existence of a lake possible, and allows for easier channel incision. This may explain why the phenomenon is not seen in other natural dams, such as landslide dams for example.

Sediment	1	2	3	4
Play Sand	1/9	1/14	2/19	1/12
Beach Sand	2/16	1/19	2/14	2/16
Grit	X	1/6	X	X

Table 3: Experimental results for the individual sediments. The columns show different experimental runs. The first number in each column is the number of waves that needed to be initiated for dambreak. The second number is the total number of waves that overtopped the dam before incision occurred. The onset of incision is taken to be the point at which the lake drains independently of the action of the seiche wave. A cross denotes a dam which did not break.

Mixture	1	2	3	4
1	X	2/28	1/15	1/8
2	1/13	1/5	2/24	1/13

Table 4: Experimental results for the sediment mixtures. The table is laid out as Table 3 above.

3 Theory

In this section, we split the problem in two. Firstly, we model the seiche wave in the lake using shallow water theory in one dimension. We then use a hydraulic model for the dambreak itself, before considering a unified theory to explain the interaction between the seiche wave and the dam.

3.1 Describing the seiche wave

We work in two dimensions, x and z. Water of velocity $\mathbf{u} = (u(x,z,t), w(x,z,t))$ and depth $h(x,t)$ flows over an erodible bed with elevation $\zeta(x,t)$. We assume that the horizontal extent of the flow is much greater than its depth; the lake is much longer than it is deep. In this case, we have that $\frac{\partial}{\partial z} \gg \frac{\partial}{\partial x}$, and thus the continuity equation implies that $u \gg w$. Conservation of vertical momentum then implies that the pressure is hydrostatic to leading order, and irrotationality that u is independent of z.

We therefore write conservation of mass and horizontal momentum in the following form

$$h_t + (hu)_x = 0, \tag{1}$$

$$u_t + uu_x = -g(h+\zeta)_x - D(u,h) + \nu u_{xx}, \tag{2}$$

where u is the depth averaged velocity, given by

$$u = \frac{1}{h}\int_{\zeta}^{h+\zeta} u\, dz, \tag{3}$$

and $D(u,h)$ is a drag term which represents frictional effects, with the properties that

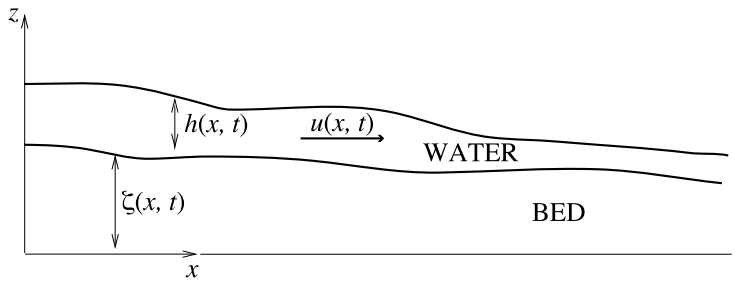

Figure 3: The co-ordinate system used in the shallow water theory.

$\frac{\partial D}{\partial u} > 0$ and $\frac{\partial D}{\partial h} < 0$; drag increases with velocity and decreases with depth. A full derivation of the shallow water equations may be found in Stoker [18], for example.

In fluvial systems, it is common to use the Chèzy drag law, given by

$$D(u,h) = c_f \frac{u|u|}{h}, \tag{4}$$

where c_f is the dimensionless Chèzy drag coefficient. Typically, for a smooth watercourse such as a glass tank, $c_f = \mathrm{O}(10^{-3})$ [1], while for a rough watercourse, such as a rocky alpine stream, it may be as large as 0.1 [6].

However, this formula is not appropriate to use in the context of our experiments, where the flow was observed to be laminar. In 1959, Keulegan determined that for a standing wave in a glass rectangular tank, the drag is primarily accounted for by laminar viscous boundary layers on the tank walls and base [10]. This theory was later modified to account for the effects of surface tension and surface contamination [12], but we shall consider these to be small corrections.

To modify Keulegan's linear theory for our purposes, we note that shallow water theory can also be used in the boundary layers near the tank walls. Using the same arguments as above, we write conservation of momentum as

$$u_t = -\frac{1}{\rho} p_x + \nu u_{zz}, \tag{5}$$

and then, given that $p_z \approx 0$, we eliminate the hydrostatic pressure to obtain

$$u_{zt} = \nu u_{zzz}. \tag{6}$$

We then pose a time periodic solution of the form $u = f(z)e^{i\omega t}$ (and consider only the real part of this solution) to obtain

$$f = C + A_{\pm} e^{\pm K z}, \tag{7}$$

where $A_{\pm}$ and C are constants of integration, and $K = \sqrt{\frac{\omega}{2\nu}}(1+i)$. The boundary conditions are

$$u_z \to 0, \qquad \text{as} \;\; \mathrm{z} \to \infty, \tag{8}$$

$$u \to u_0, \qquad \text{as} \;\; \mathrm{z} \to \infty, \tag{9}$$

$$u = 0, \qquad z = 0, \tag{10}$$

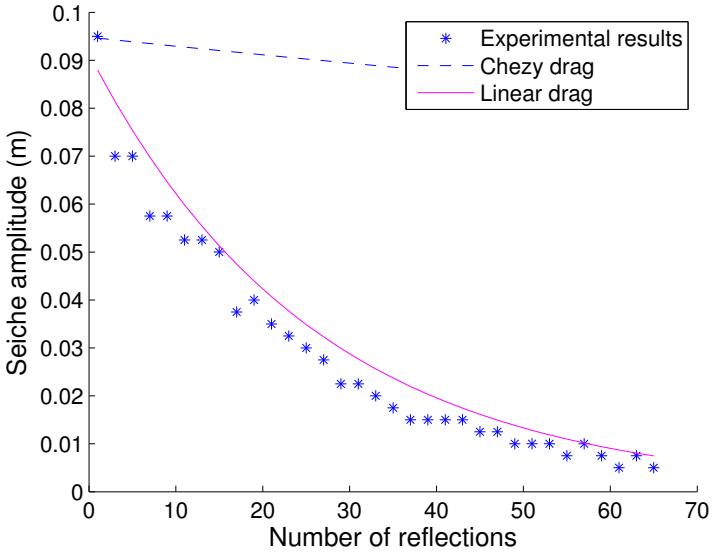

Figure 4: Comparison of the Chèzy and linear drag laws with experiment, where a seiche (standing) wave was initiated in a rectangular tank. The values used were $c_f = 0.001$, $\nu = 1 \times 10^{-6}$. We see that the linear drag theory (solid magenta line) is a much better fit to the data than the nonlinear Chèzy drag law (dashed line). Stars denote the experimental data.

where u_0 is the flow velocity in the main body of fluid outside the boundary layer. The solution is therefore

$$u = u_0 e^{i\omega t}(1 - e^{-Kz}), \tag{11}$$

and the vertical velocity gradient at the base is given by

$$u_z|_{z=0} = K u_0. \tag{12}$$

In the shallow water equations for the main flow, we therefore have

$$u_t + u u_x = -g(h + \zeta)_x - \sqrt{\frac{\nu\omega}{2}}\frac{u}{h} + \nu u_{xx}, \tag{13}$$

where the drag term is now $D(u, h) = \sqrt{\frac{\nu\omega}{2}}\frac{u}{h}$. We set $\alpha = \sqrt{\frac{\nu\omega}{2}}$; thus α has units of velocity.

We illustrate the difference between the drag laws by comparing them with the results from a simple laboratory experiment (figure 4), where a standing wave was initiated in a closed, rectangular glass tank. Figure 4 shows that that the linear drag is a much better fit to the data than the Chèzy drag; we therefore use linear drag in the theory that is to follow. However, we note that in a glacial lake where the Reynolds numbers are much higher, it is likely that the Chèzy formula will be more appropriate.

We consider a lake with mean depth $H(x)$, on which there is a seiche wave of amplitude $\eta(x, t)$, such that the total water depth is given by $h(x, t) = H(x) + \eta(x, t)$. Equations (1)

and (2) then become

$$\eta_t + [(H+\eta)u]_x = 0, \tag{14}$$

$$u_t + uu_x = -g(H+\eta+\zeta)_x - \alpha\frac{u}{h} + \nu u_{xx}. \tag{15}$$

We now nondimensionalise using the following scales

$$t \sim \frac{1}{\omega}, \quad u \sim U, \quad \eta \sim N, \quad H \sim H_0, \quad h \sim H_0, \quad \zeta \sim H_0, \quad x \sim L, \tag{16}$$

where ω is the frequency of the seiche wave. Equations (14) and (15) become

$$\omega N\eta_t + \frac{UH_0}{L}[(H+\varepsilon\eta)u]_x = 0, \tag{17}$$

$$\omega U u_t + \frac{U^2}{L}uu_x = -\frac{gH_0}{L}(H+\varepsilon\eta+\zeta)_x - \alpha\frac{U}{H_0}\frac{u}{H+\varepsilon\eta} + \nu\frac{U}{L^2}u_{xx}, \tag{18}$$

where $\varepsilon = \frac{N}{H_0} \ll 1$. To retain a balance in equation (17), we choose $U = \varepsilon\omega L$, and we assume that $(H+\zeta)_x = 0$, i. e. the undisturbed free surface is flat, to obtain,

$$\eta_t + (Hu)_x = -\varepsilon(\eta u)_x, \tag{19}$$

$$u_t + \beta\eta_x = -\varepsilon uu_x - \varepsilon\hat{\alpha}\frac{u}{H+\varepsilon\eta} + \varepsilon\hat{\nu}u_{xx}, \tag{20}$$

where the dimensionless parameters are given by

$$\beta = \frac{gH_0}{\omega^2L^2}, \quad \hat{\alpha} = \frac{\alpha}{\omega H_0}, \quad \hat{\nu} = \frac{\nu}{\omega L^2}, \tag{21}$$

and we have rescaled the drag and viscosity terms with ε; i. e. we have assumed that they are small.

We now assume that there are a fast and a slow timescale in the problem, such that $\frac{\partial}{\partial t} = \frac{\partial}{\partial \hat{t}} + \varepsilon\frac{\partial}{\partial T}$. On dropping the $\hat{}$, equations (19) and (20) become

$$\eta_t + (Hu)_x = -\varepsilon(\eta u)_x - \varepsilon\eta_T, \tag{22}$$

$$u_t + \beta\eta_x = -\varepsilon uu_x - \varepsilon\frac{\alpha u}{H+\varepsilon\eta} + \varepsilon\nu u_{xx} - \varepsilon u_T. \tag{23}$$

We now pose expansions in the form $u \sim u_0 + \varepsilon u_1 + \ldots$ and $\eta \sim \eta_0 + \varepsilon\eta_1 + \ldots$. To leading order, equations (22) and (23) are

$$\eta_{0t} + (Hu_0)_x = 0, \tag{24}$$

$$u_{0t} + \beta\eta_{0x} = 0. \tag{25}$$

Differentiating equation (24) with respect to time and using equation (25), we obtain the single equation for the wave height, η:

$$\eta_{0tt} = \beta(H\eta_{0x})_x. \tag{26}$$

In the simple case of a rectangular tank of constant depth H_0 and width L, such that the scaled boundaries are at $x = 0$ and $x = 1$, (where we require the velocity to vanish, so $\eta_x = 0$ if we assume time periodic solutions), there are solutions of the form

$$\eta = Ae^{it} \cos\left(\frac{x}{\sqrt{\beta}}\right), \tag{27}$$

where we require $\pi = \sqrt{\beta}$, i. e. $\omega = \frac{\pi\sqrt{gH_0}}{L}$. In dimensional terms, the solution for η is

$$\eta = Ae^{i\omega t} \cos\left(\frac{\pi x}{L}\right). \tag{28}$$

This first approximation to the behaviour of the seiche wave will be used in Section 3.3 below.

Numerical solutions for a given basal topography

It is possible to solve equation (26) numerically for a given basal topography, if we again assume time periodic solutions. We replace the right hand boundary, previously a vertical tank wall, by a non-erodible dam of prescribed shape, so that dimensionlessly $H = 0$ at $x = 1$. As this is an eigenvalue problem, we require three boundary conditions. On the left boundary, $x = 0$, we require that $u = 0$. At $x = 1$ (where $H = 0$) we require that the solution is regular. For the case of a uniformly sloping base, an analytic solution may be found in terms of Bessel functions, such that $\eta \sim J_0(x^{1/2})$ [19]. This analytic solution is shown in figure 5. We set $y = 1 - x$, such that close to $x = 1$,

$$\eta \sim J_0[(1-y)^{1/2}] \sim 1 + O(1-y). \tag{29}$$

To ensure we obtain a regular solution, we therefore require that $\eta = 1$ at $x = 1$. We note that near $x = 1$, $H \sim -(1-x)H'_*$, where $H'_* = H'|_{x=1}$. Again setting $y = 1 - x$, we use equation (26) to write

$$-\omega^2\eta = \beta H'_* \left(y\eta'\right)', \tag{30}$$

which gives, to leading order,

$$\omega^2\eta = \beta H'_*\eta'. \tag{31}$$

The three boundary conditions are therefore

$$\eta = 0 \qquad \text{on} \quad x = 0, \tag{32}$$

$$\eta = 1 \qquad \text{on} \quad x = 1, \tag{33}$$

$$\omega^2\eta = \beta H'_*\eta' \qquad \text{on} \quad x = 1. \tag{34}$$

Note that if $H'_* = 0$, the problem is ill-posed, as boundary conditions (33) and (34) then imply both $\eta = 0$ and $\eta = 1$ at $x = 1$. A numerical solution of equation (26) with boundary conditions (32) – (34) for a dam of Gaussian shape is shown in figure 6.

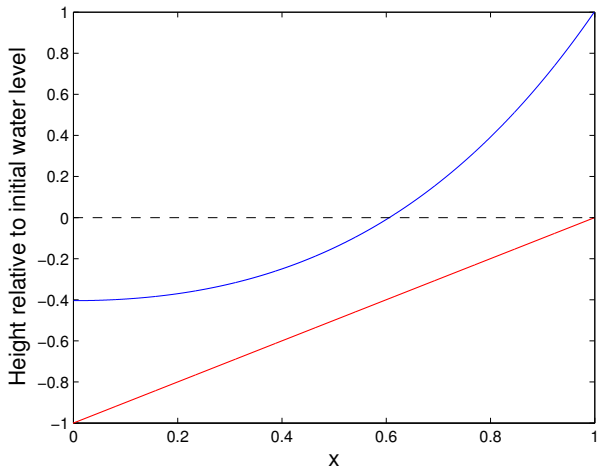

Figure 5: Numerical result for a uniformly sloping bed, with initial water depth given by $H(x) = 1 - x$. The upper solid line is the water surface, the lower line the basal topography. The dashed line indicates the initial water level.

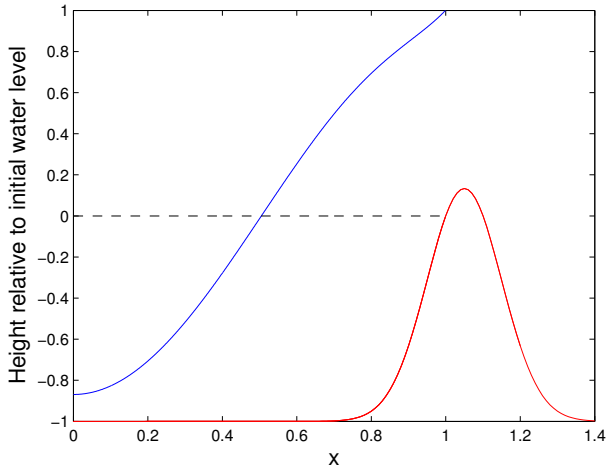

Figure 6: Numerical result for a uniformly sloping bed, with initial water depth given by $H(x) = 1 - 1.1 \exp\left(-(x - 1.05)^2/(2 \times 0.1^2)\right)$. The upper solid line is the water surface, the lower line the basal topography. The dashed line indicates the initial water level.

Higher order terms

We consider solutions of equation (26) of the form

$$(\eta_0, u_0) = (N, iU)A(T)e^{i\omega t} + \text{c.c.}, \tag{35}$$

thus N, U are real. Equations (24), (25) and (26) then become

$$\begin{aligned} \omega N &= -(HU)_x, && (36)\\ U &= \beta N_x, && (37)\\ -\omega^2 N &= \beta (H N_x)_x, && (38) \end{aligned}$$

with solutions as above. To the next order in ε, we then have

$$\begin{aligned} \eta_{1t} + (Hu_1)_x &= -(\eta_0 u_0)_x - \eta_{0T}, && (39)\\ u_{1t} + \beta \eta_{1x} &= -u_0 u_{0x} - \frac{\alpha u_0}{H} + \nu u_{0xx} - u_{0T}. && (40) \end{aligned}$$

We now use equation (35) to write equations (39) and (40) in terms of N and U;

$$\begin{aligned} \eta_{1t} + (Hu_1)_x &= -iA^2 NU e^{2i\omega t} - A_T N e^{i\omega t} + \text{c.c.} && (41)\\ u_{1t} + \beta \eta_{1x} &= A^2 U U_x e^{2i\omega t} - 2AA^* U U_x - \frac{\alpha i A U e^{i\omega t}}{H} + i\nu A U_{xx} e^{i\omega t} - i A_T U e^{i\omega t} + \text{c.c.} && (42) \end{aligned}$$

We can find particular solutions to remove any terms on the right hand sides of equations (41) and (42) which are not multiples of $e^{i\omega t}$. The remaining parts which are proportional to $e^{i\omega t}$ are potentially secular in time, and must therefore be removed in order to find a uniform asymptotic approximation over the fast time t. Discarding the non-secular inhomogeneous terms, and assuming that $\eta_1 = \eta_1(x) e^{i\omega t}$ and $u_1 = u_1(x) e^{i\omega t}$, the system we therefore look to solve is

$$\begin{aligned} i\omega \eta_1 + (Hu_1)_x &= -A_T N e^{i\omega t} && (43)\\ i\omega u_1 + \beta \eta_{1x} &= -\frac{\alpha i A U e^{i\omega t}}{H} + i\nu A U_{xx} e^{i\omega t} - i A_T U e^{i\omega t}. && (44) \end{aligned}$$

Equations (43) and (44) may be rewritten as

$$\begin{aligned} i\omega \eta_1 + (Hu_1)_x &= I_1, && (45)\\ i\omega u_1 + \beta \eta_{1x} &= I_2, && (46) \end{aligned}$$

where

$$\begin{aligned} I_1 &= -A_T N, && (47)\\ I_2 &= -\frac{\alpha i A U}{H} + i\nu A U_{xx} - i A_T U. && (48) \end{aligned}$$

We combine equations (45) and (46) to obtain

$$\omega^2 \eta_1 + \beta \left(H \eta_{1x} \right) = -i\omega I_1 + (H I_2)_x, \qquad (49)$$

and then integrate equation (49) with respect to x. After integrating by parts and using the seiche equations (36) and (37), we obtain

$$\int_0^1 N \left[-i\omega I_1 + (H I_2)_x \right] dx = 0, \qquad (50)$$

which can be simplified using equations (47) and (48) to give

$$-2A_T \int_0^1 \omega N^2 \, dx + \alpha A \int_0^1 N U_x \, dx + \nu A \int_0^1 N (H U_{xx})_x \, dx = 0. \tag{51}$$

This then gives a solution of the form $A = A_0 e^{-\gamma T}$, where γ is evaluated numerically using equation (51). The calculation can be repeated for dissipative terms given by Chèzy drag and viscosity, yielding

$$A_T \int_0^1 \omega N^2 \, dx = -\nu A \int_0^1 N (H U_{xx})_x \, dx + \frac{4A|A|c_f}{\pi} \int_0^1 N (U|U|)_x \, dx. \tag{52}$$

Again, the integrals in equation (52) may be evaluated numerically for any given basal topography $H(x)$, and this allows the relative importance of the dissipative terms to be quantified.

3.2 Modelling the dambreak

Erosion

The flux of sediment is governed by a (dimensionless) critical value of the Shields stress, defined by

$$\tau_* = \frac{u_*^2}{RgD}, \tag{53}$$

where $R = \frac{\rho_s - \rho_l}{\rho_l}$ is the specific gravity, D is a typical particle diameter and u_* is the threshold velocity, which is particular to the sediment and is determined empirically. The idea is that the fluid flow needs to exceed the threshold velocity in order to exert enough shear stress at the base to lift particles into suspension and thereby erode the bed.

We follow Parker [20], [21] and use the following empirical, dimensionless erosion law

$$E(u) = \begin{cases} \left(\frac{u^2}{u_*^2} - 1\right)^{1.5} & \text{for} \quad u > u_*, \\ 0 & \text{for} \quad u < u_*. \end{cases} \tag{54}$$

A law of this type captures the two important features of any erosion law: below a certain threshold, there is no erosion, and for large values of the Shields stress (or velocity, in this case), erosion has a power law behaviour. The exponent in equation (54) is again empirically determined and, while not universally agreed upon, it is common to use the value 1.5 [14].

In fluvial systems, the Exner equation (conservation of sediment) is commonly used to model the erosion of the dam (which has elevation $\zeta(x,t)$),

$$(1 - \lambda_p) \frac{\partial \zeta}{\partial t} + \frac{\partial q_s}{\partial x} = 0, \tag{55}$$

where λ_p is the sediment porosity and q_s is the sediment flux, which is again determined empirically as a function of the Shields stress.

However, it is also possible to consider the evolution of the dam height to be the net effect of erosion and deposition,

$$\frac{\partial \zeta}{\partial t} = -wE(u) + w_s C, \tag{56}$$

where the first term on the right hand side of equation (56) represents erosion and the second represents deposition. w is a sediment-dependent constant with units of velocity, w_s is a particle settling velocity, and C is a depth-averaged volumetric sediment concentration. Equation (56) must then be supplemented with an equation to describe the evolution of C, and it is usual to use an advection-diffusion equation, moderated by erosion and deposition, thus

$$h(C_t + uC_x) = \kappa h C_{xx} + wE(u) - w_s C, \tag{57}$$

where κ is the sediment diffusivity. As a first approximation, we assume there is no deposition; thus we eliminate C and simply use

$$\frac{\partial \zeta}{\partial t} = -wE(u). \tag{58}$$

We calculated w experimentally using equation (58), and performing erosion experiments where we measured the dam height, ζ (at a fixed point in space as a function of time), and the flow velocity u. We followed Parker [14] and calculated u_* using the following empirical relationship for τ_*

$$\tau_* = 0.5\left[0.22Re_p^{-0.6} + 0.06 \times 10^{-7.7Re_p^{-0.6}}\right], \tag{59}$$

where Re_p is the particle Reynolds number, defined as

$$Re_p = \frac{(RgD)^{1/2} D}{\nu}. \tag{60}$$

Equation (59) coupled with equation (53) allows estimation of u_* and thus w. Typical values for the sediments used experimentally are given in Table 5. It is much more complicated to estimate sediment parameters for a mixture of sediments, and so this was not attempted. For calculations involving particle diameter (such as estimation of the particle Reynolds number), the modal particle size was used.

Sediment	Re_p	τ_*	u_* (m s^{-1})	w (m s^{-1})
Play sand	20	0.0198	9×10^{-3}	9.6×10^{-9}
Beach sand	107	0.0169	1.5×10^{-2}	4.7×10^{-8}
Grit	147	0.0179	1.7×10^{-2}	4.9×10^{-8}

Table 5: Empirically and experimentally determined sediment properties.

Hydraulic Control

We now use a hydraulic model coupled with erosion to describe the dambreak. Hydraulic models are commonly used to describe stratified flows over sills in the ocean, see Pratt [15], for example. The benefit of using such a model is that at one or more locations in the system the flow adjusts to a well-defined state; i. e. it is in some sense 'controlled' by this critical point. Here, the location of hydraulic control will be the point at which the dam height is a maximum.

Hydraulic control theory also assumes steady flow. From equation (58), we have that the timescale over which erosion occurs is $t_E \sim \frac{H}{wE_0}$. Using typical values from Table 5, $u_* = 1 \times 10^{-2}$ m s^{-1} and $w = 5 \times 10^{-8}$ m s^{-1}, and a typical experimental value $H = 0.1$ m, we estimate that $t_E \approx 100$ s. This implies that for the dambreak $\frac{\partial}{\partial t} \ll 1$, and we can therefore neglect the time derivatives in the shallow water equations (1) and (2). As a first approximation, we also neglect drag and viscosity (although it is possible to include these in the description, see Pratt [15], Hogg and Hughes [7]).

We can therefore integrate the equations for conservation of mass and momentum with respect to x to obtain

$$q = hu, \tag{61}$$

$$\frac{1}{2}u^2 + g(h + \zeta) = B, \tag{62}$$

where q is the constant water flux (with units m^2 s^{-1}) and B is the energy, sometimes referred to as the Bernoulli constant.

We consider the problem of a reservoir of depth H and length L, which must drain over a dam of maximum height ζ_m. Here, the subscript $_m$ will be used to denote evaluation of a function at this maximum of ζ; thus u_m is the flow velocity at the highest point of the dam. We assume that the dam has finite width, and thus $\zeta = 0$ outside some finite region. We can therefore use equations (61) and (62) to write

$$B = \frac{1}{2}\frac{q^2}{H^2} + gH \approx gH, \tag{63}$$

if we assume that the depth of the reservoir is much greater than the depth of the water flowing over the dam, i. e. $H \gg h$. Using equation (61), we may write the non-integrated momentum equation in the form

$$u_x = \frac{-g\zeta_x u^2}{u^3 - gq}, \tag{64}$$

and thus for the velocity gradient to be defined at all points in the system, we require that $u^3 = gq$ at the point where $\zeta_x = 0$; i. e. where $\zeta = \zeta_m$. We therefore obtain

$$u_m = (gq)^{\frac{1}{3}}, \qquad h_m = \frac{q}{u_m} = \left(\frac{q^2}{g}\right)^{\frac{1}{3}}. \tag{65}$$

Note that we can use the expressions in equation (65) to write the Bernoulli constant as

$$B = \frac{3}{2}u_m^2 + g\zeta_m. \tag{66}$$

Equations (63) and (66) allow us to relate upstream variables to those at the maximum height of the dam,

$$gH = \frac{3}{2}u_m^2 + g\zeta_m. \tag{67}$$

To complete the system, we couple equations (61) and (62) with equations describing the drainage of the lake,

$$L\frac{dH}{dt} = -q, \tag{68}$$

and the erosion of the dam,

$$\frac{\partial \zeta}{\partial t} = -wE(u). \tag{69}$$

Nondimensionalisation

We nondimensionalise the system of equations (61), (62), (68) and (69) using the following scales

$$u \sim u_0, \quad h \sim h_0, \quad H \sim H_0, \quad \zeta \sim H_0, \quad t \sim t_0, \quad q \sim q_0, \quad E \sim E_0. \tag{70}$$

and thus obtain

$$\left(\frac{q_0}{h_0 u_0}\right) q = hu, \tag{71}$$

$$\frac{1}{2}\frac{u_0^2}{gH_0}u^2 + \left(\frac{h_0}{H_0}\right) h + \zeta = B^*, \tag{72}$$

$$\left(\frac{LH_0}{q_0 t_0}\right) \frac{dH}{dt} = -q, \tag{73}$$

$$\left(\frac{H_0}{wt_0 E_0}\right) \frac{\partial \zeta}{\partial t} = -E(u), \tag{74}$$

where B^* is the dimensionless Bernoulli constant.

We make the choices $q_0 = h_0 u_0$, and as we are interested in the timescale over which erosion occurs, we choose $t_0 = \frac{H_0}{wE_0}$. Equations (71) – (74) then become

$$q = hu, \tag{75}$$

$$\frac{1}{2}F^2\alpha^2 u^2 + \alpha h + \zeta = B^*, \tag{76}$$

$$\mu \frac{dH}{dt} = -q, \tag{77}$$

$$\frac{\partial \zeta}{\partial t} = -E(u^2), \tag{78}$$

where the dimensionless parameters are the Froude number, $F^2 = \frac{u_0^2}{gH_0}$, the ratio of the water height at the dam peak to the reservoir height, $\alpha = \frac{h_0}{H_0}$, and a measure of how quickly erosion occurs relative to lake drainage, $\mu = \frac{wLE_0}{q_0}$. We now make the further choices $h_0 = H_0$ and $u_0 = \sqrt{gH_0}$, such that $\alpha = F^2 = 1$.

The dimensionless form of the erosion law (equation (61)) is

$$E(u) = (u^2 - \delta^3)_+^{1.5}, \tag{79}$$

where $E_0 = \left(\frac{u_0}{u_*}\right)^3$, $\delta = \frac{u_*}{u_0}$ and the subscript $_+$ indicates that $E = 0$ when the quantity in the brackets is less than zero.

We take typical experimental values: $H_0 = 0.1$ m, $w = 5 \times 10^{-8}$ m s^{-1}, $L = 1$ m, $u_0 = 1$ m s^{-1} and $u_* = 1 \times 10^{-2}$ m s^{-1}, to obtain

$$\mu = 0.5, \quad \delta = 10^{-2}, \quad E_0 = 1 \times 10^5. \tag{80}$$

Again, we estimate $t_0 = 100$ s, which should be both the timescale for erosion and for lake drainage in our experiments (as μ is $O(1)$).

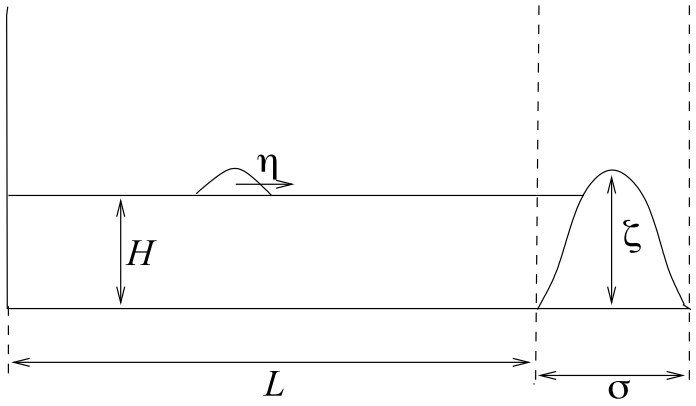

Figure 7: Schematic diagram of the two domains under consideration: a lake of length L and depth H adjacent to a dam of width σ and height ζ, such that $\sigma \ll L$ and, initially, $H \sim \zeta_m$.

3.3 Unified theory: spatially distributed dam

In order to combine the theory of the seiche wave (outlined in Section 3.1) with the hydraulic model, we consider the following configuration, shown in figure 7: a rectangular lake of length L and mean level $H(t)$, on which there is a seiche wave of amplitude $\eta(x,t)$. The lake is adjacent to a dam of height $\zeta(x,t)$ and width σ, where $\sigma \ll L$.

We now revisit the scalings used Sections 3.1 and 3.2. In the lake,

$$h = H + \varepsilon\eta, \quad t \sim \frac{1}{w} \sim \frac{\sqrt{gH_0}}{L}, \quad x \sim L, \quad u \sim \varepsilon\sqrt{gH_0}, \tag{81}$$

while over the dam,

$$t \sim \frac{H_0}{wE_0}, \quad x \sim \sigma, \quad u \sim \sqrt{gH_0}. \tag{82}$$

We impose the condition that the timescale in the lake must be of the same order as that over the dam. However, we note that velocities in the lake are $O(\varepsilon)$ smaller than those over the dam, which means that the dam 'sees' the seiche wave as a gradual change in water depth, to which it can adjust instantaneously. We also note that x derivatives are much larger over the dam than in the lake.

We assume that there is a right hand boundary of the lake which lies close to the edge of the dam, $x = x_{\sigma-}$, such that $\zeta(x_{\sigma-}, t) = 0$. We consider the water height at this fixed point, given dimensionally by $h(x_{\sigma-}, t) = H(x_{\sigma-}, t) + \eta(x_{\sigma-}, t)$, and we suppose that $\eta(x_{\sigma-}, t) = \eta(t)$ satisfies the ordinary differential equation

$$\ddot{\eta} + \gamma\dot{\eta} + \omega^2\eta = 0, \tag{83}$$

where $\gamma = \frac{\alpha}{H}$ is the damping coefficient calculated in Section 3.1, and $\omega(H)$ is the seiche frequency. As we assume that the lake is a rectangular basin, we have that $\omega = \dfrac{\pi\sqrt{gH}}{L}$ and thus $\gamma = \gamma(H)$.

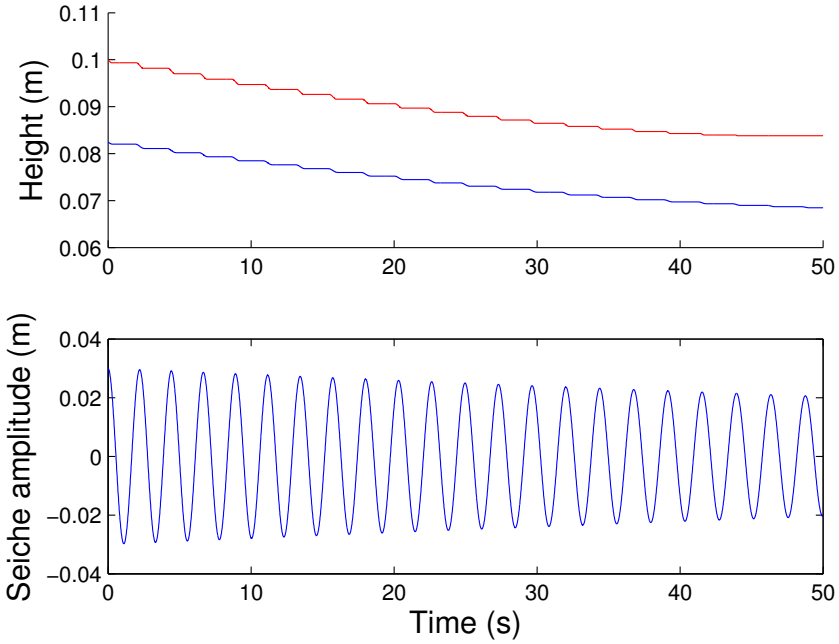

Figure 8: Solution of the spatially distributed system in the case of no dambreak, with initial conditions $\eta_0 = 0.03$ m, $H_0 = 0.0825$ m, $\zeta_0 = 0.01$ m. In the top plot, the upper (red) line shows the evolution of the maximum height of the dam, ζ_m, while the lower (blue) line shows the lake depth, H. We see that in this case there is no dambreak, as the lake level never exceeds the maximum height of the dam. The top plot shows that after approximately 42 s, erosion switches off while drainage continues; however, the velocities attained by the fluid are below the threshold and thus erosion cannot occur. The bottom graph shows the corresponding decay of the seiche amplitude.

We couple equation (83) with equations (62), (68) and (69); these are four equations for the four variables η, H, ζ and u. Numerical solutions to this system are shown in figures 8 – 10. We see that by changing the initial water depth, H_0, (and thus the initial level of the lake below the dam), we change from a regime where dambreak is possible to one where it is not. This motivates the following attempt to identify the parameters in the system which govern this threshold behaviour.

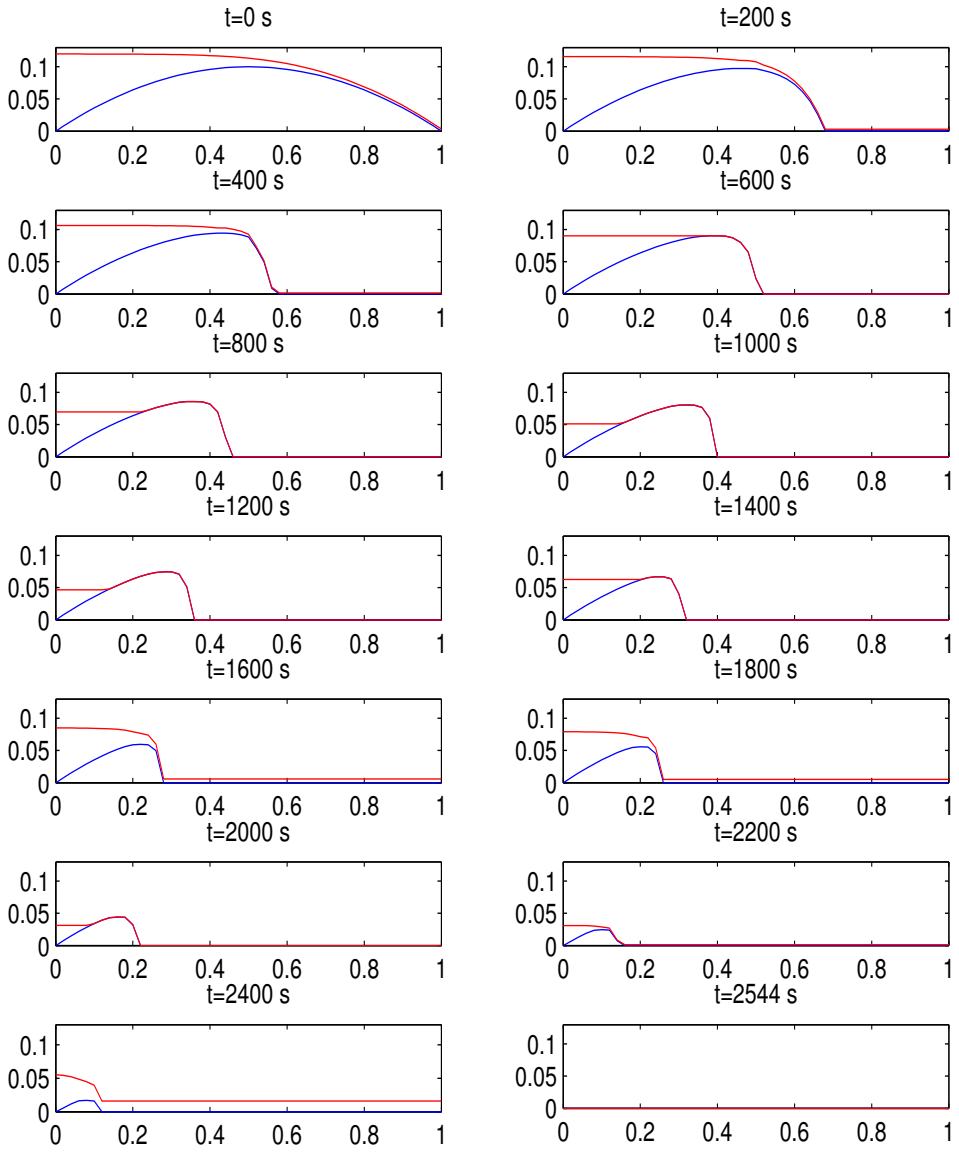

Figure 9: Snapshots of the solution in the case of dambreak, with initial conditions $\eta_0 = 0.03$ m, $H_0 = 0.09$ m, $\zeta_0 = 0.01$ m. The upper (red) line is the water level, h; the lower (blue) line the dam surface, ζ. For all graphs, the x axis is position and the y axis height. The initial dam elevation is a parabola with endpoints at $x = 0$ and $x = 1$. The solution is shown at time intervals of 200 s, and then at the time when the dam has completely eroded away (2544 s). Note the steepening of the downstream face of the dam as erosion progresses. This solution has 50 evenly spaced gridpoints.

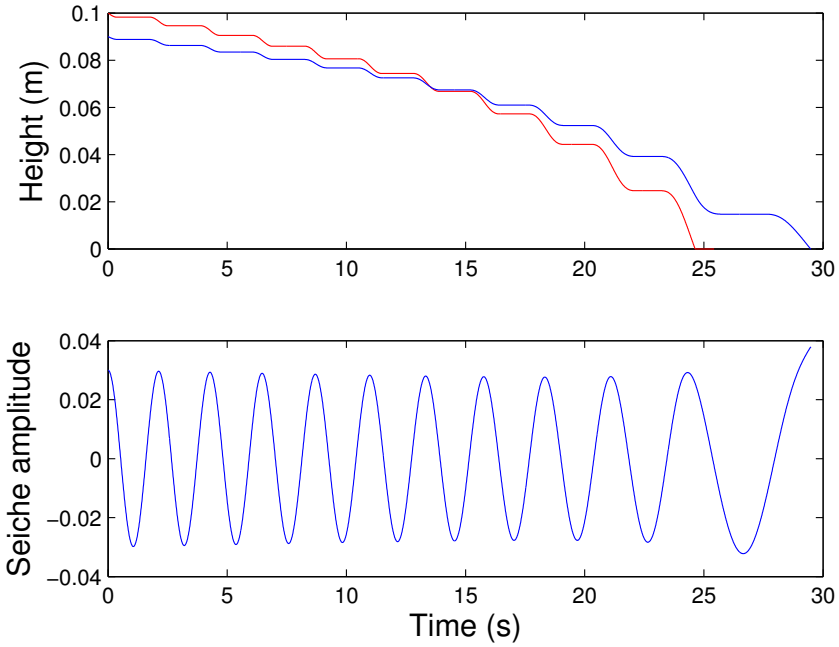

Figure 10: Solution in the case of a dambreak, for initial conditions $\eta_0 = 0.03$ m, $H_0 = 0.09$ m, $\zeta_0 = 0.01$ m (corresponding to figure 9). In the top plot, the (red) line, which is the line that is initially upper, shows the evolution of the maximum height of the dam, ζ_m, while the lower (blue) line shows the lake depth H. This plot shows erosion events, followed by periods of inactivity when the water level drops below the dam, and neither drainage nor erosion can occur. After seven such events $H > \zeta_m$, but drainage is still modulated by the seiche wave. The bottom graph shows the seiche amplitude. We note that as H becomes small so must ω, and to compensate for this, the amplitude of the seiche wave must increase.

3.4 Unified theory: point dam

To understand the governing parameters in the problem, we make a further simplification and assume that the dam can be approximated by a point, at which $\zeta = \zeta_m$. This reduces the model to the dimensional system

$$\ddot{\eta} + \gamma\dot{\eta} + \omega^2\eta = 0, \tag{84}$$

$$L\frac{dH}{dt} = -q = -\frac{u_m^3}{g}, \tag{85}$$

$$\frac{d\zeta_m}{dt} = -wE(u_m), \tag{86}$$

$$u_m = \left[\frac{2g}{3}(H + \eta - \zeta_m)\right]^{1/2}. \tag{87}$$

Equation (87) motivates the definition of a new variable, $\theta = H + \eta - \zeta_m$. Thus when $\theta > 0$ the height of the water in the lake is greater than the height of the dam, so the lake can drain over the dam. When $\theta > \theta_*$ (corresponding to the threshold velocity for erosion, u_*), erosion can occur. For $\theta < 0$, the water level is below the dam and neither drainage nor erosion can occur.

Using this definition of θ, we write equation (87) as

$$u_m = \left(\frac{2g}{3}\theta\right)^{1/2}, \tag{88}$$

and combine equations (84) and (85) to obtain a single ordinary differential equation for θ

$$\dot{\theta} = w\tilde{E}(\theta) - D\theta^{3/2} + \dot{\eta}, \tag{89}$$

where $D = \frac{1}{gL}\left(\frac{2g}{3}\right)^{3/2}$ is a drainage parameter (with units of velocity) and $\tilde{E}(\theta) = E\left[\left(\frac{2g}{3}\theta\right)^{1/2}\right]$. If we consider that H is approximately constant, then we can write the solution for the seiche wave in the form

$$\eta = \eta_0 e^{-\gamma t}\sin\omega t. \tag{90}$$

In this case, θ can be evaluated as a function of time, as shown in figure 11. We see that there are time intervals over which drainage can occur; i. e. where $\theta > 0$, and marginally shorter intervals where $\theta > \theta_*$ and erosion can occur. Erosion acts to increase these time intervals (by decreasing ζ_m and thus θ), while drainage and damping act to reduce these time intervals (by decreasing H and η respectively). We therefore see that there is a competition between erosion, which acts to increase θ, and lake drainage and seiche damping, which act to decrease θ.

This allows us to identify five parameters in the problem: the initial values θ_0 and η_0, the drainage parameter D, the erosion parameter w and the parameter governing the damping of the seiche wave, γ. We see from figure 11 that decreasing θ_0 (the initial difference between the mean lake level and the dam height) and increasing the initial seiche amplitude η_0 will

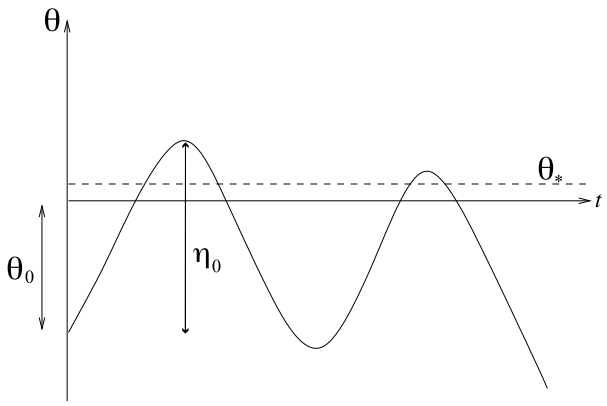

Figure 11: Schematic diagram of $\theta = H + \eta - \zeta_m$ as a function of time. When $\theta > 0$, drainage may occur, and when $\theta > \theta_*$, erosion switches on. Initially, $\eta = 0$ (from equation (90)), and thus θ_0 is simply $(H - \zeta_m)|_{t=0}$. At time $t \approx \frac{\pi}{\omega}$, $\theta \approx H + \eta_0 - \zeta_m$.

both act to increase the intervals over which erosion and drainage can occur, and thus increase the likelihood of a dam break - which is what one might intuitively expect. To investigate these parameters further, we use a difference method to crudely approximate the derivatives in equations (84) – (87). More specifically, if

$$\frac{dy}{dt} = f(y, t), \tag{91}$$

we use a difference scheme (essentially the forward Euler method) to write

$$y_n = y_{n-1} + \Delta t f(y_{n-1}, t_{n-1}), \tag{92}$$

where Δt is the time interval over which we consider the change in y. In terms of our model, we let n be the number of erosion 'events' i. e. time intervals over which $\theta > 0$. Then we set $\Delta t = T_{n-1}$, where T_{n-1} is the time interval over which the $(n-1)$th erosion event occurs.

Using figure 11, it can be estimated that

$$T_{n-1} = \frac{\pi}{\omega_{n-1}} - \frac{2}{\omega_{n-1}} \sin^{-1}\left(\frac{\zeta_{n-1} - H_{n-1}}{\eta_{n-1}}\right), \tag{93}$$

where $\omega_{n-1} = \frac{\pi\sqrt{gH_{n-1}}}{L}$. The system is now

$$\eta_n = \eta_{n-1} e^{-\frac{2\pi\gamma_n}{\omega_n}}, \tag{94}$$

$$H_n = H_{n-1} - T_{n-1}\frac{u_{n-1}^3}{gL}, \tag{95}$$

$$\zeta_n = \zeta_{n-1} - wT_{n-1}E(u_{n-1}), \tag{96}$$

$$u_n = \left[\frac{2g}{3}\left(H_n + \eta_n - \zeta_n\right)\right]^{1/2}. \tag{97}$$

Equations (93)–(97) may be solved numerically. Figure 12 shows a comparison between results from this model and those of the spatially distributed model outlined in Section 3.3 above. We see that there is agreement between the models, indicating that the simple discretised model may be sufficient to estimate the critical values of the governing parameters.

We have now answered the question posed initially regarding threshold behaviour of this system - in the context of this simple model, at least. Understanding such behaviour is useful in terms of hazard mitigation. For example, many moraine dams in the Cordillera Blanca are drained by artificial channels [8]. Figure 12 allows an estimate to be made of how low the lake level should be in order that no reasonably sized wave can break the dam.

We also wish to use our model to estimate the peak discharge of a drainage flood. The hydraulic model gives the 'weir formula' for the discharge,

$$q = \left(\frac{2}{3}\right)^{3/2} g^{1/2}(H - \zeta_m)^{3/2}, \tag{98}$$

which is simply obtained from equations (61) and (65). We compare this formulation with the experimentally determined flux. Figure 13 shows time series of water depth in a lake which drained by catastrophic erosional incision. The smaller tank width of 5 cm was chosen to prevent channelization occurring; channels formed in the 20 cm wide tank.

We used the data from figure 13 to estimate the maximum value of $\frac{dH}{dt}$. Using a value $L = 1$ m, we were then able to estimate the maximum value of q using equation (77). This value was then multiplied by the width of the lake. To use the weir formula, we estimated the maximum value of $H - \zeta_m$ during the experiment. We then multiplied this value by the width of the channel (5 cm in both cases, as the channel which formed in the 20 cm wide tank also had approximately this width).

Thus we obtain, for the narrow tank,

$$Q_{\text{data}} = 1 \times 10^{-4}\ \text{m}^3\text{s}^{-1}, \qquad Q_{\text{weir}} = 1 \times 10^{-4}\ \text{m}^3\text{s}^{-1}.$$

while for the wide tank,

$$Q_{\text{data}} = 4 \times 10^{-4}\ \text{m}^3\text{s}^{-1}, \qquad Q_{\text{weir}} = 1 \times 10^{-3}\ \text{m}^3\text{s}^{-1}.$$

We see that the predictions agree in the case of the narrow tank, but there is an overestimation of the peak discharge by the weir formula in the case of the wide tank. This may be due to our approximation of the channel as a breach of constant width.

We can compare the weir formula with empirically derived estimates of the peak discharge. Clague and Evans [2], for example, give

$$Q \sim Q_0(\lambda)\left(gd^5\right)^{1/2}, \qquad \lambda = \frac{kV}{\left(gd^7\right)^{1/2}},$$

where d is the breach depth, k is the rate (speed) of breach growth and V is the lake volume. We see that, in the case of a square breach, the weir formula would also have a $d^{5/2}$ dependence, indicating that a simple hydraulic model may capture some elements of the flood well. However, the dynamics of the channel are missing from the model, and will undoubtedly play an important role.

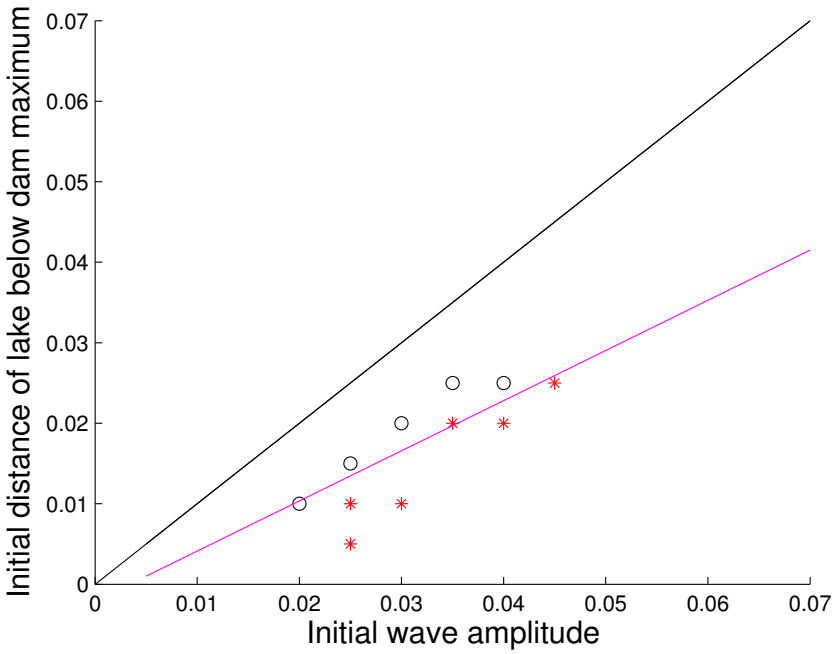

Figure 12: Comparison of the discretised point dam model with the spatially distributed model. We fix all parameters and vary only the initial wave amplitude η_0 and the initial distance between the mean water level in the lake and the dam, $(H - \zeta_m)\,|_{t=0}$. Above the upper (black) line we are in the physically unrealistic regime where η_0 is too small to overtop the dam: in this case, catastrophic incision will never occur. The lower (magenta) line indicates the results from the difference model: above this line, there is no dam break. This makes physical sense, as it implies that decreasing η_0 makes it more difficult to break the dam, while increasing the initial lake level makes it easier. On top of this are plotted results from the spatially distributed model: (red) stars indicate parameter values where incision occurred; (black) circles where it did not. We see that there is agreement between the models, although more numerical simulations using the spatially distributed model should be performed.

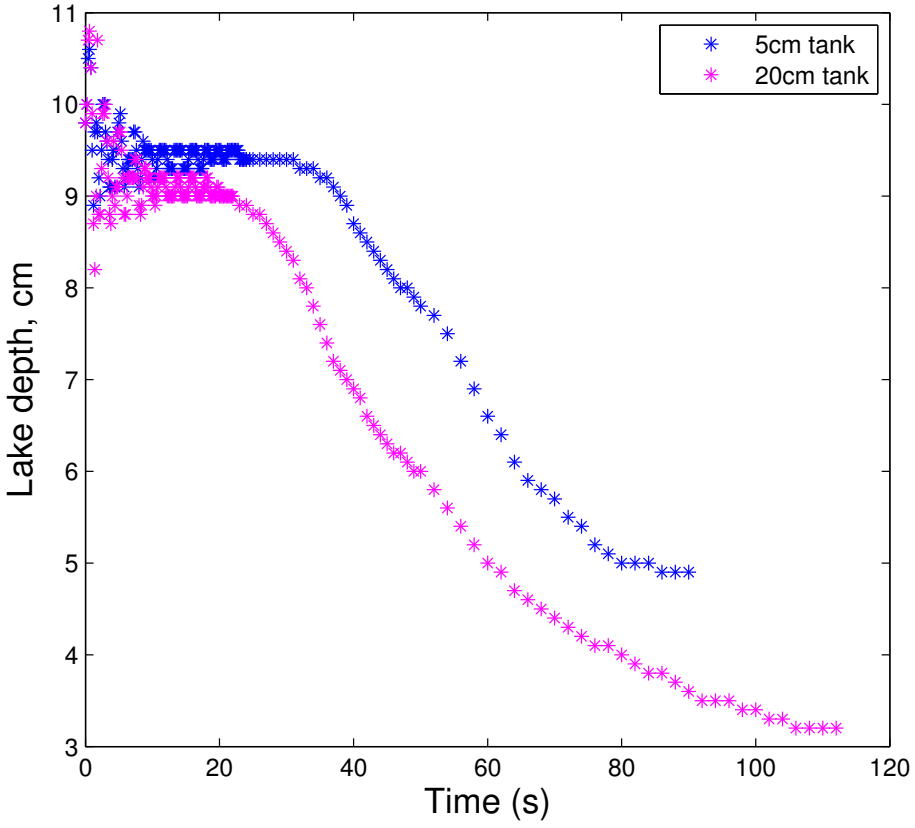

Figure 13: Time series of $H(t)+\eta(t)$ for experiments performed in a 5 cm wide tank (upper blue stars) and a 20 cm wide tank (lower magenta stars). The initial fluctuations in the data are due to the seiche wave.

4 Conclusions and future work

In this project, we have formulated and solved a one dimensional model to try and understand the breaking of a moraine dam by a mechanism which we term catastrophic erosional incision. We have seen that, experimentally, dissipation of the seiche is accounted for by linear drag and that the dambreak can be described using a hydraulic model. On joining these two simple theories together, we are able to make some rough estimates of the threshold behaviour of the phenomenon. These estimates agree qualitatively with experimental results.

Experimentally, we have confirmed the applicability of a linear damping law for the seiche wave. We have seen that the bimodal particle size distribution of moraine may explain why moraine dams are prone to fail in such a spectacular fashion: the combination of large boulders and fine sands makes the dam stable, but the loose consolidation means that it is also easily eroded. We have also compared a theoretical formulation of the peak discharge with experiment.

However, there is much future work to be done. The first step would be to include deposition in the model, as this is observed to occur experimentally. For example, as the dam erodes in the numerical simulation (figure 9), the downstream face of the dam steepens. However, experimentally the downstream face is much shallower, and the dam never erodes away completely: a dam of constant, shallow downstream slope (and approximately one quarter of the original height) remains. This final shape can perhaps be explained by the effects of deposition. Modelling this would involve either using the Exner formulation or incorporating the depth-averaged volumetric sediment into the model as described in Section 3.2.

Improvements could also be made in the description of the interaction between the seiche wave and the dam. We can use numerical methods, such as those described in Section 3.1, to allow for a more realistic basal topography. The seiche mode for such a topography, as shown in figure 6, can be coupled with a 'runup' law [19] to describe how far the seiche wave moves up the dam, and thus allow for a better coupling of the one dimensional seiche theory with the hydraulic model.

The next important step is to add an extra spatial dimension to the model in order to study the channelization instability and understand the channel dynamics. Even a basic understanding of the channel dynamics would allow for a better estimate of the peak discharge to be made. Figure 14 shows an experiment when four channels formed initially on the downstream face of the dam; two of these channels were incised to a sufficient depth to drain the lake, and did so simultaneously. It is therefore clear understanding the channelization process is key to understanding these catastrophic drainage events. Comparison can be made with the channelization instability of a flowing sheet over an erodible bed (Smith-Bretherton model, [17]), whereby a thicker layer of water acts to increase erosion, and thus deepen a channel. It should be noted, however, that in its original form such a model is mathematically ill-posed.

Finally, there is scope for more experimental exploration of some of the ideas here - a test of the results in figure 12, for example, where more accurate measurements than those obtained in our experiments would be required. Experiments could also be useful in helping to understand the channel dynamics.

Figure 14: Photograph from laboratory experiments, flow is from top to bottom. Here two channels (one on the far left, one on the far right) are draining the lake (located at the top of the picture) simultaneously. Four channels formed initially on the downstream face of the dam.

Acknowledgements

Firstly, I would like to thank Neil Balmforth for his help and patience this summer - I have certainly learned a lot! Thanks also to Keith Bradley for his 'amazing' work in the lab, and to both John and Neil for organising such an enjoyable and educational summer. Finally, thanks to the GFD staff and fellows for being so friendly (and patient on the softball field). A special thankyou must go to the monkey for the pep talks and last-minute computer wizardry.

References

[1] Baines P.G. and Whitehead J.A. *On multiple steady states in single-layer flows*, Physics of Fluids, 15(2) (2002), pp. 298-307.

[2] Clague J.J. and Evans S.G. *A review of catastrophic drainage of moraine-dammed lakes in British Columbia*, Quaternary Science Review, 19 (2000), pp. 1763-1783.

[3] Clarke G.K.C. *Subglacial Till: A Physical Framework for Its Properties and Processes*, Journal of Geophysical Research, 92(B9) (1987), pp. 9023-9036.

[4] Costa J.E. and Schuster R.L. *The formation and failure of natural dams*, Bulletin of the Geological Society of America, 100(7) (1988), pp. 1054-1068.

[5] Ericksen G.E., Plafker G. and Concha J.F., *Preliminary report on the geologic events associated with the May 31, 1970, Peru earthquake*, U.S. Geologic Survey Circular, 639 (1970), 25 pp.

[6] Fowler A.C., *Mathematics and the Environment*, Mathematical Institute (Oxford University), 2004, 264 pp.

[7] Hogg, A.M. and Hughes G.O. *Shear flow and viscosity in single-layer hydraulics*, Journal of Fluid Mechanics, 548 (2006), pp. 431-443.

[8] Hubbard B. et al. *Impact of a rock avalanche on a moraine-dammed proglacial lake: Laguna Safuna Alta, Cordillera Blanca, Peru,* Earth Surface Processes and Landforms, 30 (2005), pp. 1251-1264.

[9] Kershaw J.A., Clague J.J. and Evans S.G. *Geomorphic and sedimentological signature of a two-phase outburst flood from moraine-dammed Queen Bess Lake, British Columbia, Canada*, Earth Surface Processes and Landforms, 30 (2005), DOI: 10.1002/esp.1122.

[10] Keulegan G.H. *Energy dissipation in standing waves in rectangular basins*, Journal of Fluid Mechanics, 6 (1959),pp. 33-50.

[11] Mehta A. and Barker G.C. *Bistability and hysteresis in tilted sandpiles*, Europhysics Letters, 56(5) (2001), pp. 626-632.

[12] Miles J.W. *Surface-Wave Damping in Closed Basins*, Proceedings of the Royal Society of London A, 297 (1967), pp. 459-475.

[13] Miles J. W. *Harbor Seiching*, Annual Review of Fluid Mechanics, 6 (1974), pp. 17-36.

[14] Parker G. *1D sediment transport morphodynamics with applications to rivers and turbidity currents*, last updated April 13 2006, http://cee.uiuc.edu/people/parkerg/morphodynamics_e-book.htm

[15] Pratt, L.J. *Hydraulic Control of Sill Flow with Bottom Friction*, Journal of Physical Oceanography, 16 (1986), pp. 1970-1980.

[16] Rabassa J. Rubulis S. and Suarez J. *Rate of formation and sedimentology of (1976-1978) push-moraines, Frias Glacier, Mount Tronadoz (41° 10' S; 71° 53' W), Argentina*, in Schluchter C. (ed.): Moraines and varves: origins, genesis, classification. Rotterdam, Balkema (1979).

[17] Smith T.R. and Bretherton F.P. *Stability and the conservation of mass in drainage basin evolution*, Water Resources Research, 8(6) (1972), pp. 1506-1529.

[18] Stoker J.J. *Water Waves*. Interscience Publishers, New York, 567 pp. Third Edition (1957).

[19] Synolakis C.E. *The runup of solitary waves*, Journal of Fluid Mechanics, 185 (1987), pp. 523-545.

[20] Taki K. and Parker G. *Transportational cyclic steps created by flow over an erodible bed. Part 1. Experiments*, Journal of Hydraulic Research, 43(5) (2004), pp. 488-501.

[21] Taki K. and Parker G. *Transportational cyclic steps created by flow over an erodible bed. Part 2. Theory and numerical simulation*, Journal of Hydraulic Research, 43(5) (2004), pp. 502-514.